https://doi.org/10.5194/gmd-2023-244
Preprint. Discussion started: 9 January 2024

Geoscientific Model Development Discussions

Evaluating an accelerated forcing approach for improving computational efficiency in coupled ice sheet-ocean modelling

Qin Zhou[1], Chen Zhao[2], Rupert Gladstone[3], Tore Hattermann[4,5], David Gwyther[6], and Benjamin Galton-Fenzi[2,7,8]

[1]Akvaplan-niva AS, Tromsø, Norway
[2]Australian Antarctic Program Partnership, Institute for Marine and Antarctic Studies, University of Tasmania, Hobart, Australia
[3]Arctic Centre, University of Lapland, Rovaniemi, Finland
[4]Norwegian Polar Institute, Tromsø Norway
[5]Energy and Climate Group, Department of Physics and Technology, The Arctic University - University of Tromsø, Norway
[6]Coastal and Regional Oceanography Lab, School of Biological, Earth and Environmental Sciences, UNSW Sydney, Sydney, NSW, Australia
[7]Australian Antarctic Division, Kingston, Australia
[8]The Australian Centre for Excellence in Antarctic Science, University of Tasmania, Hobart, Australia

Correspondence: Qin Zhou (qin@akvaplan.niva.no)

Abstract.

Coupled ice sheet-ocean models are increasingly being developed and applied to important questions pertaining to processes at the Greenland and Antarctic Ice Sheet margins, which play a pivotal role in ice sheet stability and sea level rise projections. One of the challenges of such coupled modelling activities is the timescale discrepancy between ice and ocean dynamics. This discrepancy, combined with the high computational cost of ocean models due to their finer temporal resolution, limits the time frame that can be modeled. In this study, we introduce an "accelerated forcing" approach to address the timescale discrepancy and thus improve computational efficiency in a framework designed to couple evolving ice geometry to ice shelf cavity circulation. This approach is based on the assumption that the ocean adjusts faster to imposed changes than the ice sheet, with the ocean viewed as being in a slowly varying quasi-steady state over timescales of ice geometry change. By assuming that the ocean-induced ice draft change rate during one coupling interval can be reflected by a quasi-steady state change rate during a shortened coupling interval (equal to the regular coupling interval divided by a constant factor), we can reduce the ocean model simulation duration. We first demonstrate that the mean cavity residence time, derived from stand-alone ocean simulations, can guide the selection of suitable scenarios for this approach. We then evaluate the accelerated forcing approach by comparing basal melting response under the accelerated forcing with that under the regular forcing based on idealized coupled ice sheet-ocean experiments. Our results suggest that: the accelerated approach can yield comparable melting responses to those under the regular forcing when the model is subjected to steady far-field ocean conditions or time-varying conditions with timescales much shorter than the cavity residence time. However, it is not suitable when the timescale of the accelerated ocean conditions is not significantly different from the cavity residence time. When used carefully, the accelerated approach can be a useful tool in coupled ice sheet-ocean modelling.

https://doi.org/10.5194/gmd-2023-244
Preprint. Discussion started: 9 January 2024

Geoscientific Model Development Discussions

1 Introduction

The Antarctic Ice Sheet represents the largest source of uncertainty in projections of sea level rise, with its contribution estimated to vary from -5 to 43 cm of sea level equivalent by 2100 under high carbon emission scenarios (Seroussi et al., 2020). This uncertainty partly stems from the absence of ice sheet-ocean interactions in current sea level rise projections, which are based on stand-alone ice sheet models (Edwards et al., 2021; Seroussi et al., 2020). The interplay between the ice sheet and ocean around Antarctica is a tightly coupled process and cannot be overlooked. Ocean-driven basal melting of floating ice shelves, influenced by ocean currents and ice draft geometry, can trigger a non-linear response impacting ice-shelf buttressing, grounded ice velocity, grounding line movements, and ice sheet instabilities (Gladstone et al., 2012; Favier et al., 2014). Conversely, glacial meltwater from the ice shelves affects water mass transformation, sea ice formation and melting, alongside regional and global ocean circulation (Foldvik et al., 2004; Jourdain et al., 2017; Li et al., 2023), while subglacial drainage injection into ice shelf cavities drives strong regional melt increases (Nakayama et al., 2021; Gwyther et al., 2023) and impacts to sea ice formation (Goldberg et al., 2023). Moreover, stand-alone ice sheet models lack physically sound methods to compute basal melt rates under newly ungrounded ice (Jourdain et al., 2020). Therefore, coupled ice sheet-ocean models are essential for capturing the complexity of ice sheet-ocean interactions and thus improve sea level rise projections.

Driven by these needs, recent years have witnessed significant developments in coupled ice sheet-ocean modelling. Some studies follow the guidelines of the 1st Marine Ice Sheet-Ocean Model Intercomparison Project (MISOMIP1) on idealized domains (Asay-Davis et al., 2016; Favier et al., 2019; Zhao et al., 2022), while others are based on realistic, regionally-scaled domains like the Totten Glacier Area (Pelle et al., 2021; Van Achter et al., 2023), the Thwaites Glacier (Seroussi et al., 2017), the Filchner-Ronne Ice Shelf (Timmermann and Goeller, 2017; Naughten et al., 2021). More recently, coupled ice sheet-ocean model configurations on the circumpolar scale or beyond, with cavities explicitly resolved, have begun to emerge (Smith et al., 2021; Pelletier et al., 2022), primarily in testing phases or for sensitivity studies (Muntjewerf et al., 2021). Applying the circumpolar coupled ice-ocean models to long-term simulations is heavily constrained by the timescale discrepancy between ice and ocean dynamics. The ice sheet timescale ranges from decades to millennia, while the ocean timescale spans from hours to decades. As a result, the typical timestep sizes are smaller for ocean models (seconds to minutes) compared to those for ice sheet models (days to months), making the ocean model more computationally demanding to run. These limitations prevent the coupled models from running a longer-term and larger ensemble of simulations, both of which are important for sea level rise projections.

In this study, we introduce an approach of "time compression" or "accelerated forcing" to address the challenge of timescale discrepancy between the ocean and ice-sheet models. With this approach, the temporal scale of the ocean model is adjusted to be α times faster than the real-time temporal scale. α is referred to as the acceleration factor throughout the text. This approach shares a similar idea with the approach of a morphological acceleration factor used by the sediment transport modelling community, which effectively extends the morphological simulation duration by multiplying the changes in bed sediments by a constant factor (Lesse et al., 2004; Li et al., 2018; Morgan et al., 2020).

https://doi.org/10.5194/gmd-2023-244
Preprint. Discussion started: 9 January 2024

Geoscientific Model Development Discussions

In the context of coupled ice sheet-ocean modelling, the accelerated forcing approach is based on the assumption that the ocean adjusts faster to imposed changes than the ice sheet, with the ocean viewed as being in a slowly varying quasi-steady state over timescales of ice geometry change. Note that the quasi-steady state here refers to the phase where the ocean model maintains a consistent average response to external forcings over the timescales that matter for ice sheet geometry changes. Specifically, the oceanic effect on the ice draft change Δz_d, expressed as an integral of ice draft change rate $\dot{z_d}(t)$ over the coupling time interval T as

$$\Delta z_d = \int^{T} \dot{z_d}(t) dt, \tag{1}$$

can be linearly decomposed into the time integral of a slowly varying quasi-steady-state change rate $\overline{\dot{z_d}(t)}$ over the coupling interval as

$$\Delta z_d = \overline{\dot{z_d}(t)} \cdot T. \tag{2}$$

By assuming that the ice draft change rate $\overline{\dot{z_d}(t)}$ during the coupling interval T can be reflected by a quasi-steady-state change rate $\overline{\dot{z_d}(t/\alpha)}$ during a shortened coupling interval of T/α, the ocean model simulation duration can be reduced from T to T/α, hereby accelerating the timescale of the ocean model by a factor of α. In addition, to maintain the model's integrity under the accelerated approach, the timescales of the ocean model's boundary conditions should be also accelerated, specifically by dividing them by a factor of α, to accommodate the timescale change from T to T/α.

It is important to note that the above assumptions may not always hold true. However, our hypothesis proposes that this accelerated forcing approach remains valid under specific conditions - particularly when the quasi-steady state basal melting response is not sensitive to the boundary conditions that must be accordingly accelerated. This understanding provides a foundation upon which suitable scenarios for the approach can be determined. Specifically, it emphasizes the need to investigate how the basal melting in the ocean model responds to boundary conditions with varying timescales: the far-field ocean conditions outside of the ice shelf cavity and the ice draft change at the ice sheet-ocean interface.

The far-field ocean conditions influencing ice sheet-ocean interactions around Antarctica range from seasonal and decadal fluctuations (Dutrieux et al., 2014; Jenkins, 2016) to longer, century-scale shifts associated with climate warming (Hellmer et al., 2012; Naughten et al., 2021). Given such vast variability, the systematic testing of the feasibility of the accelerated forcing approach becomes inefficient. Nevertheless, Holland (2017) suggests that the melting to time-varying ocean forcing is dictated by the relative magnitude of two timescales, the forcing timescale and the mean cavity residence time that is the characteristic time taken for the barotropic circulation flush the entire cavity (Holland, 2017). The basal melting remains relatively stable when the cavity is subject to ocean conditions varying more rapidly than the cavity residence time, suggesting a scenario where the accelerated forcing approach might be applicable. However, the approach's applicability under ocean conditions, which vary slower than the cavity residence time, requires further experimental investigation. Following Holland (2017)'s study of exploring the melting response to time-varying ocean forcing, we will first use stand-alone ocean models to identify the suitable scenarios for pragmatically applying the accelerated forcing approach.

https://doi.org/10.5194/gmd-2023-244
Preprint. Discussion started: 9 January 2024

Geoscientific Model Development Discussions
Open Access
EGU

The study is organized as follows: Section 2 briefly introduces the implementation of the accelerated forcing approach in the coupled ice sheet-ocean system. Section 3 explores the basal melting to oscillating far-field ocean conditions to determine suitable scenarios for the accelerated approach with stand-alone ocean experiments. Section 4 evaluates the accelerated forcing approach for three scenarios with coupled ice sheet-ocean experiments with the MISOMIP1 framework. Lastly, Section 5 summarizes the findings and discusses the applicability and limitations of the approach.

2 Methodology and model description

2.1 The coupler: FISOC

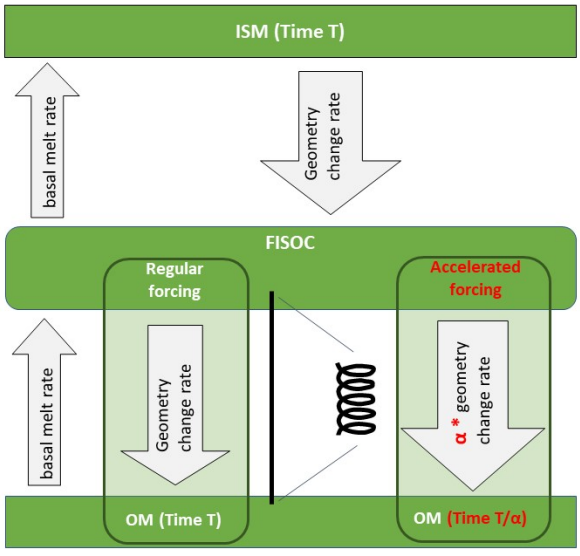

Figure 1. Data flow for the coupled ice sheet-ocean coupled system, indicating the difference between the regular forcing and the accelerated forcing approach. ISM and OM stand for ice sheet model and ocean model, respectively.

The current study implements the accelerated forcing approach within the Framework For Ice Sheet–Ocean Coupling (FISOC). This flexible coupling framework, adopting the hierarchical modular structure of the Earth System Modelling Framework, allows exchange of data between ice sheet and ocean models at the underside of the ice shelves (Gladstone et al., 2021). Figure 1 illustrates the workflow of the coupled ice sheet-ocean model system, both with and without the accelerated forcing approach. In the absence of the accelerated forcing approach as ”regular forcing” within FISOC, the basal melt rates, calculated by the ocean model, are passed from the ocean model to the ice model, while geometry change rates, determined by the ice

https://doi.org/10.5194/gmd-2023-244
Preprint. Discussion started: 9 January 2024

Geoscientific Model Development Discussions

model, are passed from the ice model to the ocean model, as

$$\frac{dz_d}{dt}_{[O]} = \frac{dz_d}{dt}_{[I]}. \tag{3}$$

Here z_d is the ice draft, and subscripts in square brackets indicate the representation of the same property within either the ice [I] or ocean [O] component. This exchange occurs at a coupling interval of T. Conversely, under the "accelerated forcing" approach with an acceleration factor α, the boundary conditions imposed by the ice sheet model on the ocean model must be adjusted accordingly. Specifically, the geometry change rates received by the ocean model are amplified by a factor of α, as

$$\frac{dz_d}{d(t/\alpha)}_{[O]} = \alpha\frac{dz_d}{dt}_{[O]} = \alpha\frac{dz_d}{dt}_{[I]}. \tag{4}$$

As the ocean model is run for a period of T/α each coupling interval instead of T, the total change in ice geometry experienced by the ocean model during one coupling interval is the same under the accelerated forcing as the regular forcing. But the computational efficiency has been increased α times. It is important to note that throughout the text, we distinguish between *model time*, which refers to the ocean model's actual simulation time (T/α for one coupling interval), and *represented time*, which signifies the real world time represented by the model, calculated as the model time multiplied by the acceleration factor (T for one coupling interval).

2.2 The ice-sheet model, Elmer/Ice

For the ice model in the coupled simulations, we use Elmer/Ice, a finite-element, dynamic ice sheet model (Gagliardini et al., 2013). Here, the SSA* solution, a variant of the L1L2 solution of Schoof (2010), is used to solve the shallow shelf approximation of the Stokes equations.The SSA* approximation accounts for longitudinal and lateral stresses with an assumption of a simplified vertical shearing in the effective strain rate to represent fast-flowing ice streams and ice shelves. The SSA* approximation was recently coupled with the ocean model ROMS using FISOC (Zhao et al., 2022), and the same configuration is used in this study. A constant surface mass balance rate of 0.3 myr^{-1} is applied here.

We assume a constant ice temperature in the ice model and zero heat flux across the ice-ocean boundary. The ice front location does not vary with time and the ice mass loss due to calving disappears immediately without any freshwater flux into the ocean. A non-linear Weertman-type sliding relationship (Eq. (21) in Gagliardini et al. (2013)) was applied for grounded ice, with a sliding parameter equal to 0.01 $\mathrm{MPam}^{\frac{1}{3}}\mathrm{a}^{\frac{1}{3}}$ and an exponent equal to $\frac{1}{3}$. The shelf regions are free slip.

2.3 The ocean models, FVCOM and ROMS

To increase the generality of our evaluations of the accelerated forcing approach, we conduct our main experiments using two different regional ocean models. The primary model is the Finite Volume Community Ocean Model (FVCOM) (Chen et al., 2003). While FVCOM is noted for its unstructured grid allowing geometric flexibility to resolve small-scale ice sheet-ocean interaction processes (Zhou and Hattermann, 2020), it is chosen here due to the authors' expertise with the model and its potential applications in future work. We also conduct selected experiments with the Regional Oceanic modelling System (ROMS) (Shchepetkin and McWilliams, 2005). ROMS employs a structured Arakawa C-grid and has been widely

https://doi.org/10.5194/gmd-2023-244
Preprint. Discussion started: 9 January 2024

Geoscientific Model Development Discussions

Table 1. Characteristics of the FVCOM and ROMS configurations used in this study.

	FVCOM	ROMS
Horizontal grid	unstructured triangle grid	structured C-grid
Horizontal discretization	finite volumes	finite differences
Horizontal mixing scheme	Eddy closure parameterization	Laplacian mixing scheme
Vertical mixing scheme	Mellor and Yamada level 2.5	K-Profile Parameterization

used for resolving ice shelf cavities around Antarctica (Dinniman et al., 2007; Naughten et al., 2018; Galton-Fenzi et al., 2012; Richter et al., 2022). In addition to different grids, the two models differ in many aspects including numerical discretization, advection schemes, and mixing scheme parameterizations. Table 1 outlines some key differences in model characteristics between FVCOM and ROMS. However, it is worth noting that both models employ terrain-following vertical coordinates and share a number of similarities in resolving ice shelf cavities, including:

- Ice shelf-ocean thermodynamics are parameterized by the three-equation formulation following Jenkins et al. (2010). Specifically, in both models, values of $Cd = 0.0025$, $\Gamma_{\mathrm{T}} = 0.05$, and $\Gamma_{\mathrm{S}} = 0.0014$ are used for the drag coefficient and the turbulent heat and salt exchange coefficients, respectively.
- Both ocean models account for the thermodynamic effect of basal melting by imposing virtual heat and salt fluxes within a fixed geometry at each ocean model time step, to mimic the effects of basal melting, rather than employing an explicit volume flux at the ice-ocean interface.
- Ice shelf mechanical pressure is given by the density at the first layer of the model minus an assumed linear dependence of the density with depth, following Dinniman et al. (2007).
- In coupled model setups, the grounding line movement is realized by the wet and dry scheme, allowing a passive water column under the grounded ice and an active water column under floating ice or in the open ocean.

3 Stand-alone ocean experiments

3.1 Experiment design

To increase the generality of our investigations of melting response to ocean forcing with varying timescales, we employ two model domains differing in ice cavity geometry for our stand-alone ocean experiments. The first, as illustrated in Figure 2, is the Ice Shelf - Ocean Model Intercomparison Project (ISOMIP+) domain (Asay-Davis et al., 2016). It features a rectangular box bounded by $320\ \mathrm{km} \leq \mathrm{x} \leq 800\ \mathrm{km}$ in the x direction and $0 \leq \mathrm{y} \leq 80\ \mathrm{km}$ in the y direction, with the initial grounding line position at $\mathrm{x} = 460\ \mathrm{km}$. The second domain features the same rectangular box but with a simplistic, wedge-shaped ice shelf in

https://doi.org/10.5194/gmd-2023-244
Preprint. Discussion started: 9 January 2024

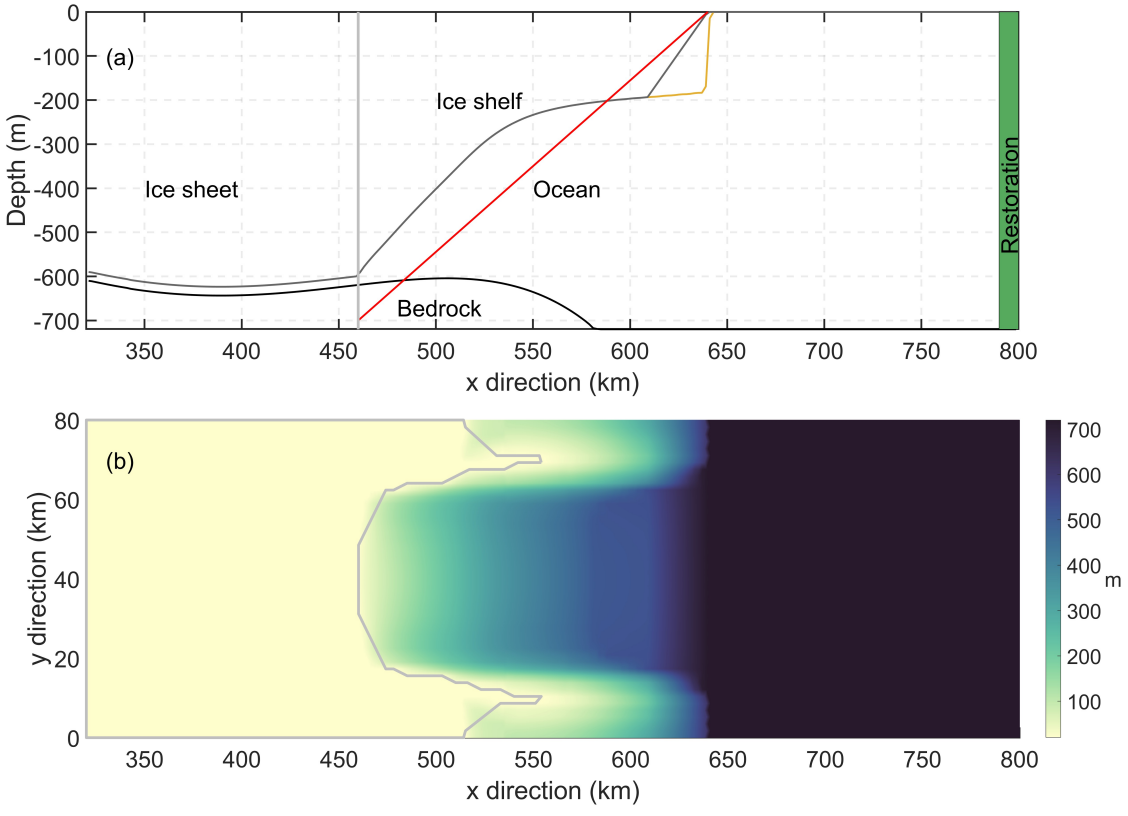

Figure 2. (a) Cross-sectional view along the center of the ISOMIP+ domain showing various key components: the bottom topography (black line), the initial grounding line position (light gray straight line), and the ice shelf geometry used in FVCOM simulations (dark grey line). Note that ROMS uses the same ice shelf geometry except at the ice front ($610\ \mathrm{km} \leq x \leq 640\ \mathrm{km}$), and the curry-color line denotes the ice front as utilized in ROMS simulations. The red line indicates the ice shelf geometry used in FVCOM simulations with the Wedge cavity. The green shaded area marks the region of far-field forcing restoration utilized by the ocean model. (b) Plain-view of the ISOMIP+ domain, with color shading indicating the water column thickness. The light grey lines denote the initial boundary separating the wet cells (to the right) and the dry cells (to the left). This ISOMIP+ domain also serves as the domain for ocean components in the coupled ice sheet-ocean experiments.

https://doi.org/10.5194/gmd-2023-244
Preprint. Discussion started: 9 January 2024

Geoscientific Model Development Discussions
Open Access
EGU

a flat-bottom ocean (Figure 2a), henceforth referred to as the "Wedge". The wedge domain is implemented only in FVCOM, resulting in three model configurations: FVCOM-ISOMIP+, FVCOM-Wedge, and ROMS-ISOMIP+.

All configurations have a horizontal resolution of 2 km. The only external forcing in the model is a restoring forcing of far-field ocean conditions within 10 km of the lateral boundary of the domain ($790\ \mathrm{km} \leq \mathrm{x} \leq 800\ \mathrm{km}$), as indicated by the green area in Figure 2a. The initial ocean properties and far-field ocean conditions consist of horizontally homogeneous temperature and salinity profiles that vary linearly with water depth:

$$T = T_0 + (T_b - T_0)\frac{z}{D} \tag{5}$$

and

$$S = S_0 + (S_b - S_0)\frac{z}{D}, \tag{6}$$

where $D = 720\ \mathrm{m}$ is the maximum water depth, and T_0, S_0 and T_b, S_b denote the surface and bottom values for temperature and salinity, respectively. Depending on the experiment, the temperature and salinity profiles used are either constant or oscillating over time. For constant profiles, as detailed in Table 2, we adopt the COLD and WARM profiles from Asay-Davis et al. (2016). These profiles represent typical ocean conditions near Antarctic ice shelves, with "COLD" and "WARM" referring to the conditions near cold and warm ice shelves, respectively. The MEAN profiles, derived by averaging the COLD and WARM profiles, qualitatively represent average ocean properties.

The oscillating profiles are conducted as repeating cosine waves, fluctuating between the COLD and WARM profiles with a period P as

$$T_P(t) = 0.5(T_W + T_C) - 0.5(T_W - T_C)cos(\frac{2\pi}{\mathrm{P}}t), \tag{7}$$

and

$$S_P(t) = 0.5(S_W + S_C) - 0.5(S_W - S_C)cos(\frac{2\pi}{\mathrm{P}}t). \tag{8}$$

Here T_P and S_P stand for the oscillating profiles for potential temperature and salinity, respectively. T_W and S_W are the linear warm profiles for potential temperature and salinity, respectively, and T_C and S_C are the linear COLD profiles for potential temperature and salinity, respectively. When averaged over the period P, these oscillating profiles yield the MEAN profiles.

Table 3 summarizes the stand-alone ocean experiments. For each configuration, we conduct three constant forcing simulations and a number of oscillating forcing simulations with different periods. Specifically, oscillation periods for FVCOM-ISOMIP+ are 0.1, 0.2, 0.6, 1, 2, 6, 10, 20, and 30 years. Periods for FVCOM-Wedge are 0.1, 0.2, 1, 2, 10, and 20 years. Periods for ROMS-ISOMIP+ are 0.4, 4, 8, 20, and 36 years. While all the constant forcing simulations are initialized from the COLD rest state, the oscillating simulations are initialized from the spun-up state of the respective COLD forcing simulations. Each simulation was run until a quasi-equilibrium state was achieved, characterized as a constant state of mean melting for the constant forcing simulations and a repetitive state for the oscillating forcing simulations. Here the quasi-equilibrium state refers to the model's spun-up phase, in which the model's outputs are no longer influenced by the initial conditions but are

https://doi.org/10.5194/gmd-2023-244
Preprint. Discussion started: 9 January 2024

Geoscientific Model Development Discussions
Open Access
EGU

Table 2. Summary of parameters for the temperature and salinity profiles. Note that all salinities on the practical salinity scale (PSS-78).

Profiles	Surface temperature, T_0	Bottom temperature, T_b	Surface salinity, S_0	Bottom salinity, S_b
COLD	-1.9°C	-1.9°C	33.8	34.55
MEAN	-1.9°C	-0.45°C	33.8	34.625
WARM	-1.9°C	1°C	33.8	34.7

Table 3. Summary of stand-alone ocean experiments.

Experiment class	Simulation name	Initial state	Restoring forcing profiles
FVCOM-ISOMIP+	FI_C2C	at rest, COLD	COLD
	FI_C2M	at rest, COLD	MEAN
	FI_C2W	at rest, COLD	WARM
	FI_P	FI_C2C spun-up state	oscillating, period P
FVCOM-Wedge	FW_C2C	at rest, COLD	COLD
	FW_C2M	at rest, COLD	MEAN
	FW_C2W	at rest, COLD	WARM
	FW_P	FW_C2C spun-up state	oscillating, period P
ROMS-ISOMIP+	RI_C2C	at rest, COLD	COLD
	RI_C2M	at rest, COLD	MEAN
	RI_C2W	at rest, COLD	WARM
	RI_P	RI_C2C spun-up state	oscillating, period P

instead determined by the external forcings. Unless stated otherwise, our analysis is based on results from a quasi-equilibrium state, which are time-averaged over the final year of model time for constant simulations and over the last cycle for oscillating simulations.

3.2 Melting response to oscillating ocean forcing

As we will explore the melting response to oscillating ocean forcing in comparison with the constant MEAN forcing, it is necessary first to examine the melting response from the simulations restored to the MEAN profiles. Throughout the text, all the measures derived from these MEAN forcing simulations are referred to as mean-state measures. Despite their different cavity geometries, the two FVCOM MEAN forcing simulations (FI_C2M and FW_C2M) exhibit similar barotropic circulation patterns, as illustrated in Figure 3a and c. Both simulations display a single clockwise gyre in the open ocean. Within the ice cavity, the circulation primarily exhibits a geostrophically controlled flow, featuring an inflow of boundary waters across the

https://doi.org/10.5194/gmd-2023-244
Preprint. Discussion started: 9 January 2024

Geoscientific Model Development Discussions

Table 4. Melting diagnostics for simulations restored to the MEAN profiles across different model configurations.

Simulation name	Cavity volume (m^3)	Cavity-averaged barotropic streamfunction (Sv)	Cavity-averaged melt rate (myr^{-1})	Mean cavity residence time (yr)
FI_C2M	3.9×10^{12}	0.03	1.87	~ 4
FW_C2M	4.6×10^{12}	0.07	2.7	~ 2
RI_C2M	3.75×10^{12}	0.018	0.97	~ 7

ice front and along the lower flank and an outflow along the upper flank. Consequently, in both FVCOM simulations, intense melting is observed near the deepest part of the lower flank, while significant freezing occurs along the upper flank (Figure 3b and d). However, the strength of the circulation and the associated melting-freezing process varies with the different ice cavity geometries. Notably, the ISOMIP+ cavity (FI_C2M; Figure 3a) exhibits much weaker circulation compared to the wedge cavity (FW_C2M; Figure 3c), highlighting the effect of cavity geometry on the circulation and, consequently, on melting patterns.

In contrast, despite using the same ISOMIP+ cavity and being restored to the same MEAN profiles, the ROMS simulation (RI_C2M) exhibits distinct barotropic circulation patterns (Figure 3e) compared to its FVCOM counterpart (FI_C2M;Figure 3a). Specifically, RI_C2M features three gyres in the open ocean and an inflow across the lower part of the ice front ($y = 0 - 20$ km), along with an anti-clockwise gyre near the ice front in the cavity. Additionally, basal melting in RI_C2M (Figure 3f) is generally weaker than that in FI_C2M (Figure 3b). It is important to note that our focus here is to understand the melting response within each model configuration to oscillating ocean forcing, rather than directly comparing the two models. The observed differences between the ROMS and FVCOM MEAN forcing simulations may reflect a combination of differences in model numerics (Table 1) and artifacts associated with the pressure gradient error (Zhou and Hattermann, 2020). The ISOMIP+ cavity ice front in the FVCOM simulation was smoothed to mitigate the pressure gradient error, unlike in the ROMS simulation, likely leading to a smaller pressure gradient error.

Table 4 presents cavity-averaged melt rates alongside with the mean-state cavity residence time (MCRT) from these three MEAN forcing simulations.The MCRT, computed by dividing the cavity volume by the cavity-averaged barotropic streamfunctions, represents the time required for all the cavity waters to be flushed with the MEAN forcing waters to fully affect the basal melting (Holland, 2017). Next we will use the MCRT as a key timescale for investigating the response of basal melting to oscillating ocean restoring conditions.

Figure 4 displays the time series of domain-averaged temperatures and cavity-averaged melt rates from selected simulations for each of the three model configurations: three constant forcing simulations (COLD, MEAN, and WARM) and three oscillating simulations with periods that are either shorter than 0.1 times the MCRT, close to or within 2 times the MCRT, or significantly longer than 5 times the MCRT. Across the three model configurations, the WARM forcing simulation displays highest temperatures and, consequently, the highest melt rates. Notably,Although the mean-state temperature is intermediate between the WARM and COLD simulations, the corresponding mean-state melt rate stays more closely with the COLD simu-

https://doi.org/10.5194/gmd-2023-244
Preprint. Discussion started: 9 January 2024

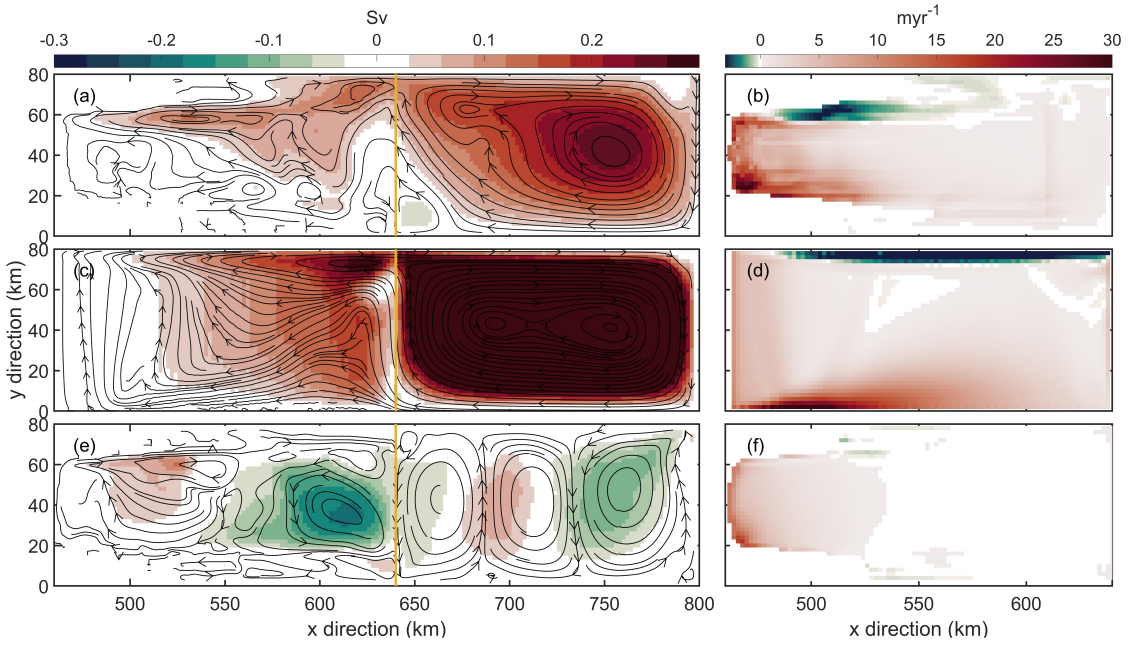

Figure 3. The left column shows plan views of the quasi-steady state barotropic streamfunction from simulations restored to the MEAN profiles for FI_C2M (a), FW_C2M (c), and RI_C2M (e), with black lines and arrows indicating the barotropic flow and the yellow line marking the ice front location. The right column presents plan views of the basal melt rates from the same simulations: FI_C2M (b), FW_C2M (d), and RI_C2M (f).

lation, rather than evenly between the two. This suggests a non-linear, possibly quadratic relation between ocean temperatures and melt rates (Holland et al., 2008).

In all the oscillating simulations, both the temperature curve and the melt rate curve exhibit oscillation patterns that reflect the periods of the respective ocean forcing. Moreover, the melt rate curves, particularly in the longer-period simulations (orange lines in Figure 4d,e,f), exhibit a distinct asymmetrical shape. Specifically, this asymmetry is characterized by broader low melt troughs, representing phases when the cavity is filled with COLD water, in contrast to narrower high melt peaks, indicative of phases with WARM water in the cavity. The asymmetry is related to the internal feedback between cavity circulation and boundary forcing (Holland, 2017). During a forcing cycle where the far-field ocean conditions vary from WARM to COLD and back to WARM, when the cavity is filled with WARM water, the enhanced melting leads to faster cavity circulation, facilitating quicker flushing of COLD water and rapid cooling of the cavity. Conversely, in a COLD cavity state, the circulation slows, extending the time taken to flush WARM water into the cavity, hence resulting in a slower warming phase. This asymmetry is also visible in the simulations with forcing periods close to the CMRT (blue lines in Figure 4d,e,f).

In Figure 4d, e, and f, the melt rate curves from simulations subjected to oscillating forcing exhibit share common features across different model configurations: i) for periods significantly shorter than the MCRT, indicated by green lines, melt rates are slightly above their respective mean-state values; ii) for periods close to the MCRT, shown by cyan lines, the majority of

https://doi.org/10.5194/gmd-2023-244
Preprint. Discussion started: 9 January 2024

Geoscientific Model Development Discussions

melt rates fall beneath the mean-state values, suggesting reduced melting in these simulations; iii) for periods substantially longer than the MCRT, as depicted by orange lines, peak or trough melt rates reach or are near those seen in the respective WARM or COLD forcing simulations, suggesting that melting is nearly in equilibrium with the periodic forcing at all times. Additionally, the majority of melt rates lie above the mean-state values.

These features are also evident in the spatial distributions of melt rate deviations from the selected oscillating simulations, relative to their respective mean-state melt rates (Figure 5). For periods significantly shorter than the MCRT (FI_0.2yr, FW_0.1yr and RI_0.4yr; top row in Figure 5), enhanced melting is mainly observed in the inner part of the cavity, with the cavity-averaged melt rates increasing by 10%, 5% and 14%. For periods close to the MCRT(FI_6yr, FW_2yr, and RI_10yr), the spatial distribution shows a significant reduction in melting at locations of strong mean-state melting, as compared with the mean-state melting pattern illustrated in Figure 3b, c, and e. The cavity-averaged melt rates decrease by 31%, 29% and 29%. For periods substantially longer than the MCRT (FI_30yr, FW_20yr and RI_36yr; bottom row in Figure 5), there is a general increase in melting, particularly in the inner part of the cavity in the two FVCOM simulations (FI_30yr and FW_20yr), with the melt rates rising by 29%, 12% and 13%.

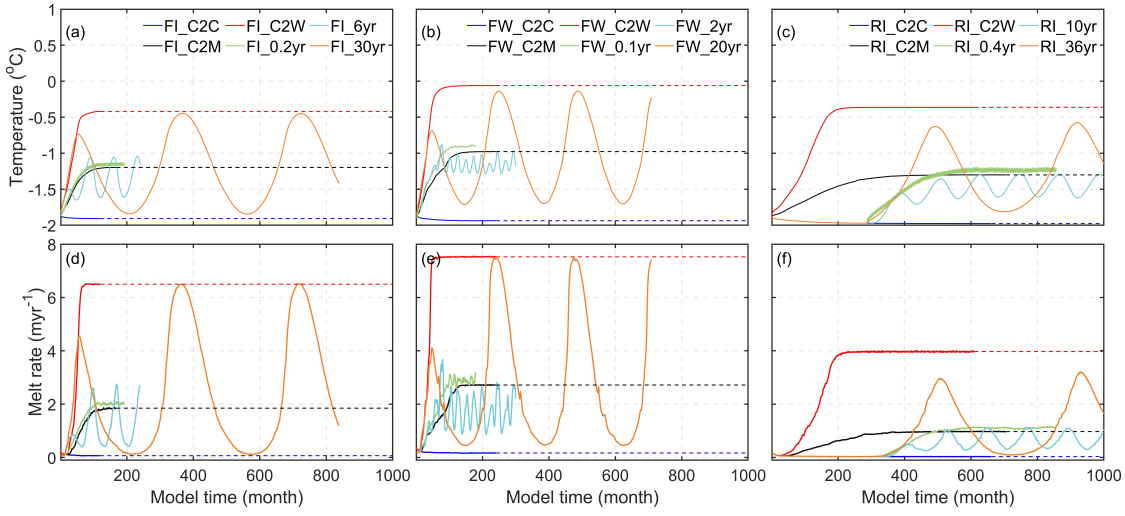

Figure 4. Time series of domain-averaged temperatures from selected simulations in configurations (a) FVCOM-ISOMIP+, (b) FVCOM-Wedge, and (c) ROMS-ISOMIP+. Time series of cavity-averaged melt rates from selected simulations in (d) FVCOM-ISOMIP+, (e) FVCOM-Wedge, and (f) ROMS-ISOMIP+. The dashed lines extend from their respective quasi-steady state values for interpretative purposes.

Figure 6 provides a qualitative summary of melting response to oscillating forcing across all the simulations in three model configurations, by depicting the relationship between normalized melt rate and normalized timescale. The normalized melt rate is computed by dividing the cavity-averaged melt rate in each oscillating forcing simulation by the corresponding mean-state cavity-averaged melt rate. Similarly, the normalized timescale is the ratio of the oscillating period to the respective MCRT. As we use Log2(Normalized timescale) for the x-axis in the figure, a value of 0 indicates a forcing oscillation period close to the

https://doi.org/10.5194/gmd-2023-244
Preprint. Discussion started: 9 January 2024

Geoscientific Model Development Discussions
Open Access
EGU

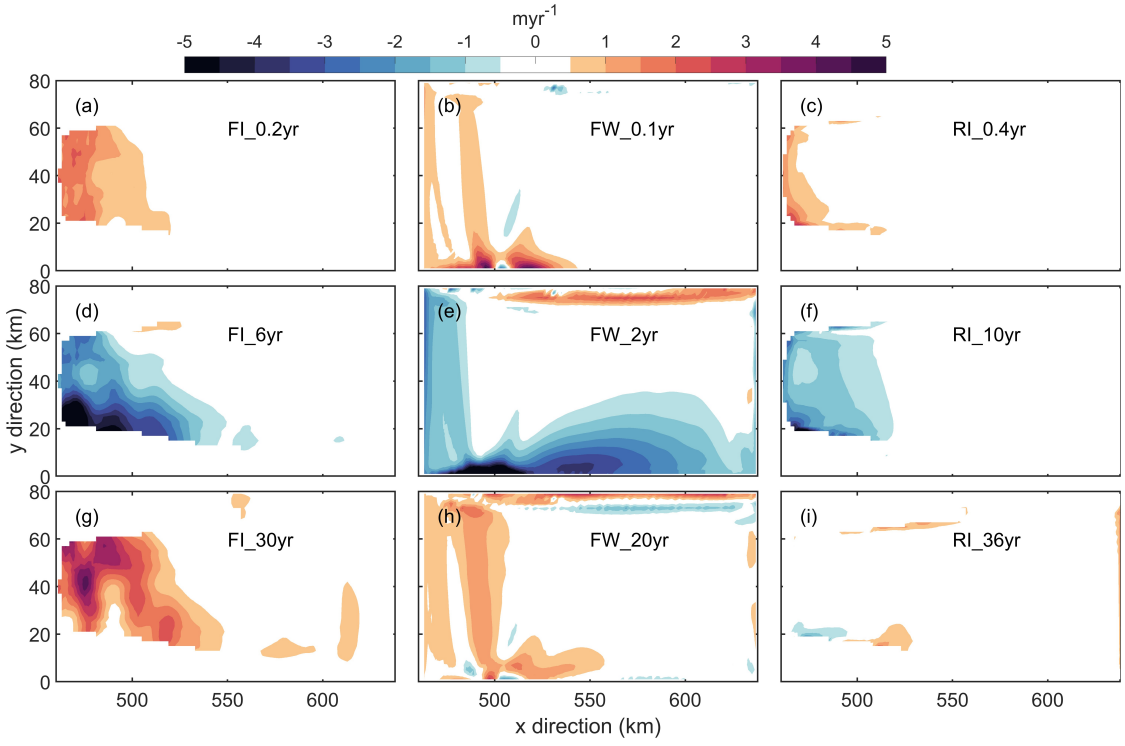

Figure 5. Spatial distributions of melt rate deviations from selected oscillating forcing simulations, relative to their respective mean-state melt rates, across the three model configurations: FVCOM-ISOMIP+ (a,d,e), FVCOM-Wedge (b,e,h), and ROMS-ISOMIP+ (c,f,i). The top, middle, and bottom rows correspond to simulations with forcing periods significantly shorter, approximately equal to, and substantially longer than their respective MCRTs.

MCRT, a value of -2 indicates a forcing period of 0.25 times the MCRT, while a value of 2 indicates a forcing period of 4 times the MCRT.

Figure 6 not only reinforces the three distinct melting regimes observed in the time series and spatial distribution figures but also provides two additional key insights crucial for determining the applicability of the accelerated forcing approach. Firstly, when oscillation periods are shorter than the MCRT (Log2(Normalized timescale) < 0), the melting rates tend to stabilize, as indicated by normalized melt rates clustering between 0.9 and 1.1. This is because multiple COLD and WARM waters coexist within the cavity in this regime, effectively canceling each other in the spatial mean, leading to a melting response close to that from the MEAN forcing simulation. Consequently, in this regime, the melting response exhibits low sensitivity to rapidly varying ocean forcing. Given our earlier assertion that the accelerated forcing approach only remains valid when basal melting response is not sensitive to corresponding accelerations in ocean boundary forcing, we deduce the approach is applicable in this regime. Secondly, all three model configurations show that normalized melt rates drop to about 0.7 for oscillation periods near the MCRTs (Log2(Normalized timescale) $\approx$ 0), marking the lowest normalized melt rates among all oscillating simulations. This suggests that any alteration in the forcing timescale, for instance, changing from Log2(Normalized timescale) $\approx$ 0 to $\approx$

https://doi.org/10.5194/gmd-2023-244
Preprint. Discussion started: 9 January 2024

Geoscientific Model Development Discussions

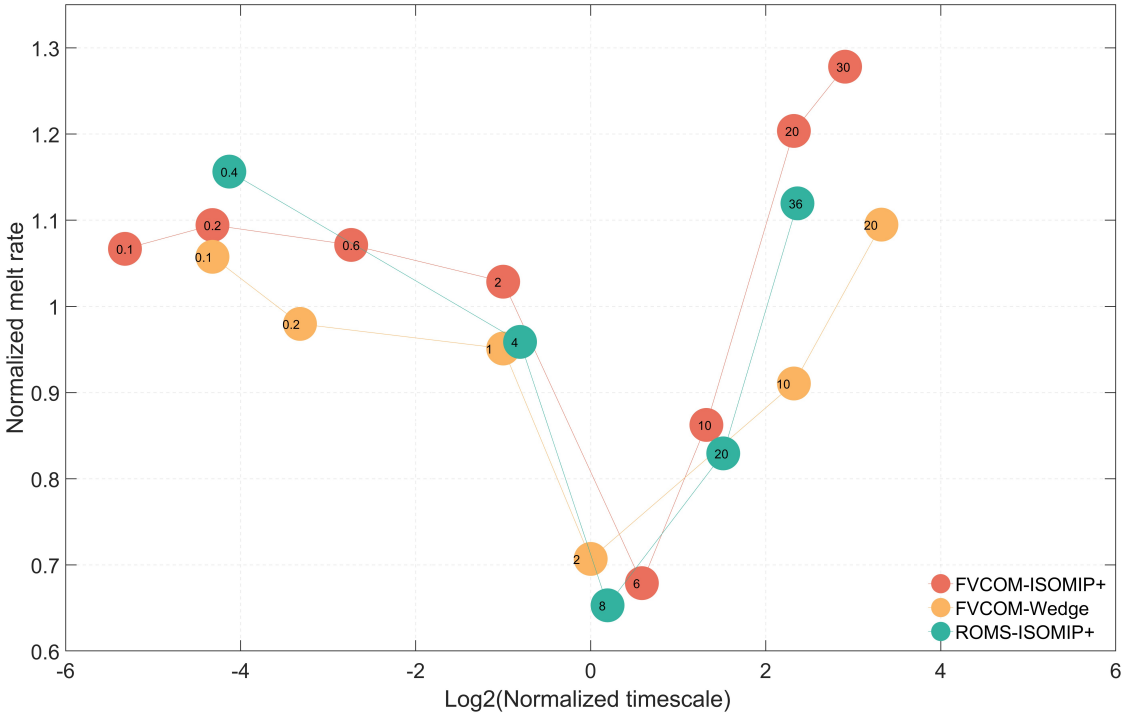

Figure 6. Normalized melt rates plotted against normalized timescales across three model configurations. The period of oscillating profiles used in each simulation is denoted by the black text within the colored circles.

2, could significantly impact the melting response. Thus, when the oscillation period of ocean forcing, whether under regular or accelerated forcing approaches, approximates the mean cavity residence time, the accelerated forcing approach may not be suitable.

In the following section, we will use coupled ice sheet-ocean experiments to verify these findings and evaluate the accelerated forcing approach.

4 Coupled ice sheet-ocean experiments

4.1 Experiment design

To explore the approach's applicability across various ocean models, we conduct our main experiments using two coupled model setups: Elmer/Ice-FVCOM and Elmer/Ice-ROMS.

Our coupled experiments are based on the MISOMIP1 IceOcean1 experiment framework (Asay-Davis et al., 2016). Accordingly, the ocean model domain is identical to the domain used in the stand-alone ocean experiments (Figure 2), while the ice sheet model domain extends from 0 to 640 km in the x direction. We have structured the coupled experiments into three classes characterized by the timescale of far-field ocean conditions: Constant, Periodic-fast, and Periodic-slow. Each class includes

https://doi.org/10.5194/gmd-2023-244
Preprint. Discussion started: 9 January 2024

Geoscientific Model Development Discussions
Open Access
EGU

Table 5. Summary of coupled ice sheet-ocean experiments. For the Constant class, "Rest" in the simulation name indicates the simulation is initialized from the COLD rest state, while "Spunup" indicates the simulation is initialized from the quasi-steady state of the respective regular forcing simulation. The suffix "_R" in the simulation name denotes the use of ROMS in the coupled model. The period shown in brackets refers to model time not represented time (which is always 0.6 yr for fast and 30 yr for slow periodic forcing).

Experiment class	Simulation name	Acceleration factor	Restoring forcing profiles (period)
Constant	CRest1(_R)	1	WARM
	CRest3(_R)	3	WARM
	CRest10(_R)	10	WARM
	CSpunup3(_R)	3	WARM
	CSpunup10(_R)	10	WARM
Periodic-fast	PFast1	1	oscillating (0.6 yr)
	PFast3	3	oscillating (0.2 yr)
	PFast10	10	oscillating (0.06 yr)
Periodic-slow	PSlow1	1	oscillating (30 yr)
	PSlow1.5	1.5	oscillating (20 yr)
	PSlow3	3	oscillating (10 yr)

one benchmark simulation under regular forcing and several simulations under accelerated forcing, as listed in Table 5 and explained in detail below.

The Constant class represents a scenario where an ice shelf cavity experiences a regime shift from a cold to a warm cavity. Each coupled model setup has one regular forcing and four accelerated forcing simulations. The regular forcing simulation, identical to the COLD-to-WARM MISOMIP1 IceOcean1r experiment (Asay-Davis et al., 2016), is initialized from the COLD rest state and restored to the WARM profiles. Two accelerated forcing simulations, using acceleration factors of 3 and 10, are initialized from the COLD rest state. Another two accelerated forcing simulations, with the same acceleration factors, are initialized from the spun-up state of the respective regular forcing simulation. Specifically, the FVCOM-based spun-up state is after 144 months simulation in model time and the ROMS-based spun-up state is after 240 months simulation in model time. All accelerated forcing simulations are restored to the same WARM profiles as the regular forcing simulation. This is because the timescale of a constant forcing can be considered infinite, and any accelerations of it are also infinite. We run simulations for 1200 months in represented time. Note that we use both Elmer/Ice-FVCOM and Elmer/Ice-ROMS for this class. However, due to resource constraints, we only use Elmer/Ice-FVCOM for the following two classes.

The Periodic-fast class represents a scenario where an ice shelf cavity experiences fast-varying far-field ocean conditions with a timescale much shorter than its cavity residence time. The regular forcing simulation is restored to the oscillating profiles

https://doi.org/10.5194/gmd-2023-244
Preprint. Discussion started: 9 January 2024


Geoscientific Model Development Discussions

with a period of 0.6 years, which is significantly shorter than a MCRT of 4 years. Two accelerated forcing simulations, using acceleration factors of 3 and 10, are restored to the oscillating profiles with periods of 0.2 and 0.06 years in model time, respectively. All simulations in this class are initialized from the 240-month spun-up state of the stand-alone simulation with the MEAN profiles (FI_C2M). We run all simulations for 400 months in represented time, beyond their spin-up phase and reaching a quasi-equilibrium state.

The Periodic-slow class represents a scenario where an ice shelf cavity experiences slow-varying far-field ocean conditions that vary over a timescale significantly longer than its cavity residence time. The regular forcing simulation is restored to the 30-year period oscillating profiles, more than seven times longer than a MCRT of 4 years. Longer periods are not feasible in the current configuration due to computational constraints. Two accelerated forcing simulations, using acceleration factors of 1.5 and 3, are restored to the oscillating profiles with periods of 20 and 10 years in model time, respectively. All simulations in this class are initialized from the 600-month spun-up state of the stand-alone simulation forced with the 30-year oscillating profiles (FI_30yr). We run all simulations for 690 months in represented time.

4.2 Evaluating the accelerated forcing approach

We now evaluate the accelerated forcing approach by directly comparing key diagnostics relevant to basal melting from the corresponding accelerated forcing simulations to those from the corresponding regular forcing simulation. These diagnostics include time series of cavity-averaged melt rates and ocean volume changes, along with spatial distributions of melt rates. We also assess spatial distributions of integrated ice draft changes and grounding line positions at the end of the simulation.

4.2.1 Constant far-field ocean conditions

In the CRest simulations where the ocean model starts from the COLD rest state and undergoes the WARM forcing, the FVCOM-based coupled system takes a similar period (110 months in model time) to adjust to the transient forcing changes, whether under regular forcing or accelerated forcing (Figure 7a). During this adjustment, warmer water from the boundaries flushes into the ice cavity, causing melt rates to rise from 0–$\sim$2.4 myr^{-1} for all experiments, despite the different accelerated ice draft change rates. This pattern indicates that the spin-up duration is mainly dictated by ocean boundary conditions, not by the feedback in the coupled model system. Consequently, the melting response during the spin-up phase in the regular forcing simulation (CRest1) is not reproduced in the accelerated forcing simulations when viewed in represented time (CRest3, CRest10; Figure 7b), suggesting the accelerated forcing approach is not effective during this phase. This conclusion is supported by results from the ROMS-based setup (CRest3_R, CRest10_R to CRest1_R in Figure 7d).

In contrast, the accelerated forcing simulations initialized from a spun-up state exhibit similar temporal melting response to the regular forcing simulation. For the FVCOM-based setup, both of the two accelerated simulations (CSpunup3, CSpunup10) yield a constant melt rate of about $2.4\ \mathrm{myr}^{-1}$, nearly identical to that in the regular forcing simulation (CRest1; Figure 7b). For the ROMS-based setup, the accelerated forcing approach can effectively capture oscillations in the melt rates, which are primarily attributed to an ocean response to the ice draft changes (Zhao et al., 2022), with comparable frequency and magnitude

https://doi.org/10.5194/gmd-2023-244
Preprint. Discussion started: 9 January 2024


Geoscientific Model Development Discussions

to those under the regular forcing (Figure 7d). Thus, our subsequent analysis focuses only on the accelerated forcing simulations initialized from a spun-up ocean state.

Furthermore, the spatial pattern of basal melting from the accelerated forcing simulations closely matches that from the regular forcing simulation for the FVCOM-based setup, with minor exceptions in the deeper parts of the cavity. The spatial pattern in the regular forcing simulation (CRest1) shows enhanced melting in the deep ice region near the grounding line (x< 450 km) with a region-averaged melt rate of $24\ \mathrm{myr}^{-1}$, as shown in Figure 8a. Absolute differences in melt rates from both accelerated forcing simulations (CSpunup3, CSpunup10) relative to the regular forcing simulation are lower than $0.5\ \mathrm{myr}^{-1}$ across most of the cavity, indicated by the large uncolored areas away from the deep ice region in Figure 8c and Figure 8e. In the deep ice region, the region-averaged melt rate differences relative to the regular forcing simulation are $1.5\ \mathrm{myr}^{-1}$ and $3\ \mathrm{myr}^{-1}$ for the accelerated forcing simulations with factors of 3 and 10, respectively, both representing relative melting changes below 4%.

A similar conclusion can be drawn from the outcome of the ROMS-based coupled simulations, particularly for the lower acceleration factor, as shown in the right column of Figure 8. In specific, visible differences in melt rates from both accelerated forcing simulations (CSpunup3_R,CSpunup10_R) relative to the regular forcing simulation (CRest_R) mainly occur in the newly ungrounded high-melting region (x < 440 km; Figure 8f,h) . In this region, the accelerated forcing simulation of a factor of 3 shows an absolute difference in area-averaged melt rate of $5\ \mathrm{myr}^{-1}$, representing a relative change of 6% of the area-averaged melt rate of $79\ \mathrm{myr}^{-1}$ seen from the regular forcing simulation (Figure 8d). However, this difference increases to $43\ \mathrm{myr}^{-1}$ with an acceleration factor 10, amounting to a relative change beyond 50%. This substantial difference is likely a result of increased draft change rates interacting with the sudden alteration in ice draft slope and corresponding circulation (Zhao et al., 2022).

Time series of ocean volume changes from both FVCOM-based accelerated forcing simulations (CSpunup3, CSpunup10) also exhibit a remarkable agreement with those from the regular forcing simulation, showing a steady increase from 0 to approximately $2\times10^{12}\mathrm{m}^3$ over the represented 1200 months (as depicted in the black lines in Figure 9a). This reflects continuous mass transfer from ice to ocean under the constant WARM forcing. The ROMS-based simulations shows a similar trend, with discrepancies between the regular and the accelerated forcing remaining below 2% in the last 900 represented months (Figure 9b). Note that the peaks in the accelerated simulation curves are likely attributed to the ROMS-based system's adjustment to the accelerated ice draft change rates, with a higher factor leading to a more pronounced peak.

Additionally, the grounding line positions are consistent between the regular and the accelerated forcing simulations, located at x = 436 km and x = 431 km for the FVCOM-based and the ROMS-based setups, respectively. Deviations in integrated draft changes from the regular forcing simulation are generally small, except near the grounding line. In the FVCOM-based setup, the integrated ice draft changes in the regular forcing simulation increase from about 50 m at the ice front to approximately 350 m near the original grounding line ($\mathrm{x} \approx 460\mathrm{km}$), and then decreases to below 50 m in the newly-ungrounded area (Figure 9c). The absolute differences in ice draft changes are typically below 5 m for an acceleration factor of 3 and below 10 m for a factor of 10 across most of the cavity (Figure 9e,g). However, at certain locations near the grounding line, these differences increases to over 10 m and 20 m for factors of 3 and 10, respectively, representing relative changes exceeding 20% and 40%.

https://doi.org/10.5194/gmd-2023-244
Preprint. Discussion started: 9 January 2024

Geoscientific Model Development Discussions

In the ROMS-based setup, integrated ice draft changes in the regular forcing simulation increase from about 50 m at the ice front to over 400 m at approximately 15 km from the grounding line, and then decrease to about 100 m at the grounding line (Figure 9d). While most of the cavity exhibits small deviations similar in magnitude to the FVCOM-based counterparts, significant deviations from the regular forcing simulation in the ROMS-based setup are concentrated within 15 km to the grounding line (Figure 9 f,h). At certain locations here, the absolute differences at certain locations exceed 20 m and 50 m for factors of 3 and 10, respectively, corresponding to relative changes of more than 20% and 50%.

While there are significant deviations, exceeding 20% compared to the regular forcing simulation, in integrated ice draft changes at certain locations in the newly grounded region, our findings suggest that the accelerated forcing approach is applicable in scenarios where an ice shelf cavity experiences steady far-field ocean conditions. This is particularly true for the lower acceleration factor, evidenced by the less than 10% relative changes in integrated ice draft changes across most of the cavity, less than 2% in total ocean volume changes, and less than 6% in melt rates, while maintaining the grounding line positions when using an acceleration factor of 3 in both FVCOM-based and ROMS-based setups. However, given that the temporal melting response in the accelerated forcing simulations diverges from the regular forcing simulation during the spin-up phase, the accelerated forcing approach is only suited for the spun-up phase.

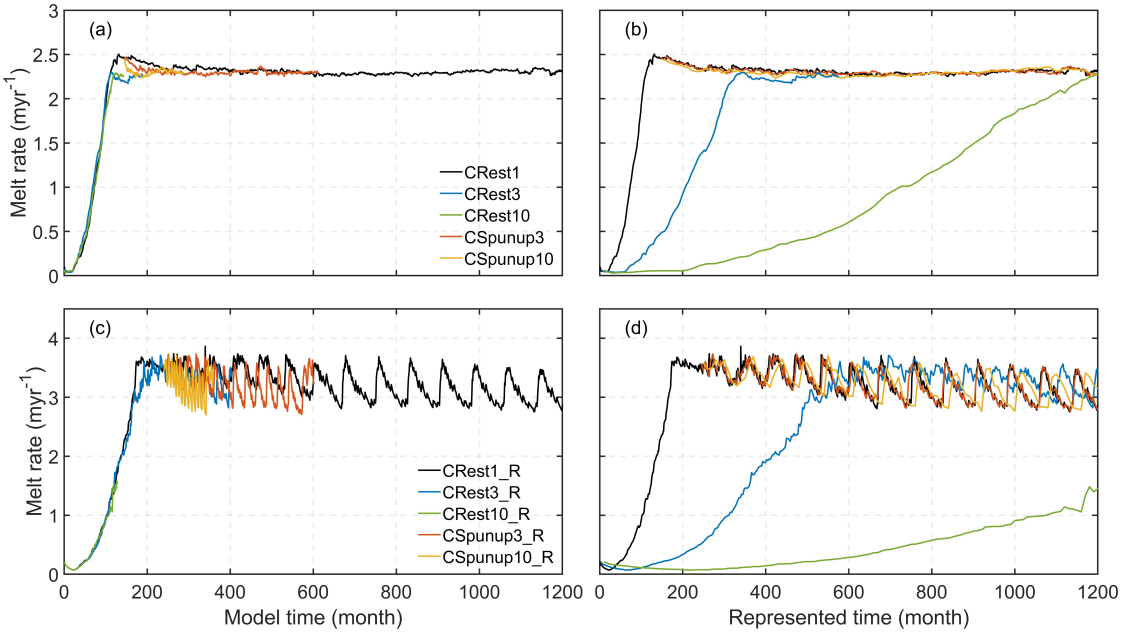

Figure 7. Time series of cavity-averaged melt rates derived from the FVCOM-based coupled simulations in terms of (a) model time and (b) represented time.Time series of cavity-averaged melt rates derived from the ROMS-based coupled simulations in terms of (c) model time and (d) represented time.

https://doi.org/10.5194/gmd-2023-244
Preprint. Discussion started: 9 January 2024

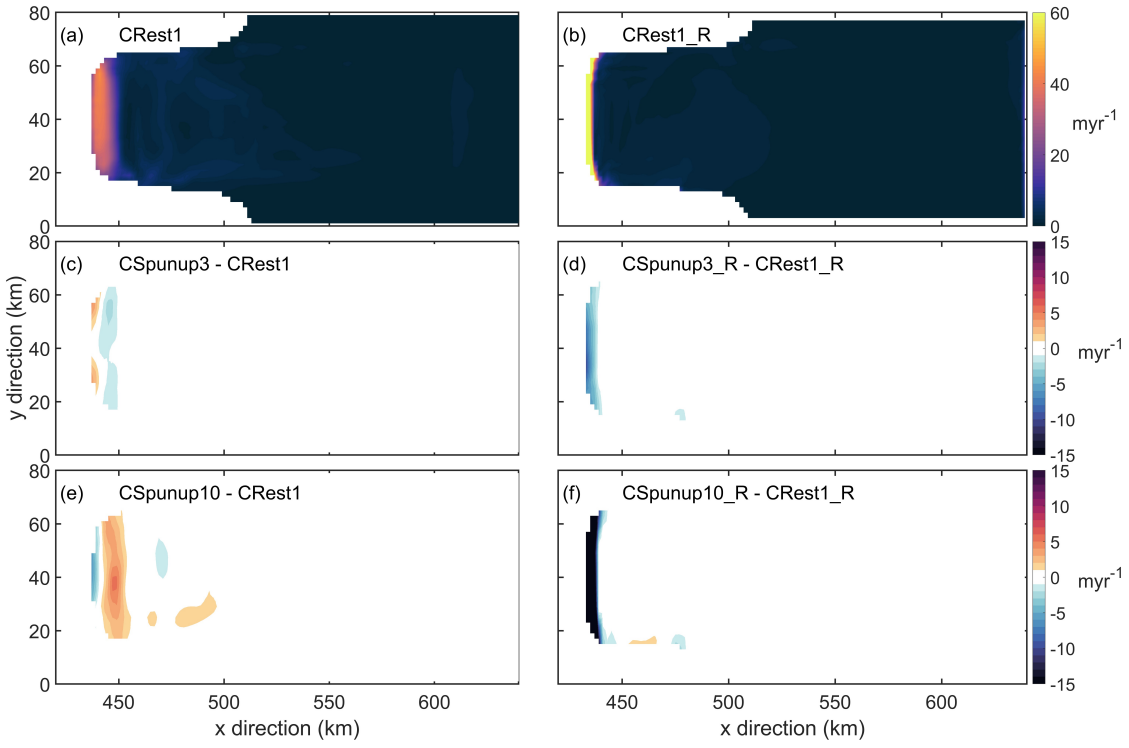

Figure 8. Panel (a) shows spatial distributions of melt rates from the FVCOM-based regular forcing simulation, and panels (c, e) show spatial distributions of difference in melt rates from both FVCOM-based accelerated forcing simulations relative to the regular forcing simulation. Panel (b) shows spatial distributions of melt rates from the ROMS-based regular forcing simulation, and panels (d, f) shows spatial distributions of difference in melt rates from both ROMS-based accelerated forcing simulations relative to the regular forcing simulation.

4.2.2 Fast-varying far-field ocean conditions

In the coupled model exposed to fast-varying ocean conditions with timescale much shorter than the MCRT, the regular forcing simulation (PFast1) shows high-frequency variability in temporal melting response, as depicted by the gray lines in Figure 10a. This variability is not captured in the accelerated forcing simulations (PFast3/10; red and orange lines in Figure 10a). However, for the evolution of the coupled ice-ocean system, the time-averaged is more important than the high-frequency variability. Across all three simulations, we see similar trends in cavity-averaged melt rates. The accelerated forcing simulations exhibit melt rates that fluctuate around the low-pass filtered time series of the regular forcing simulation (black lines; Figure 10a). The maximum deviation observed is approximately $0.1\ \mathrm{myr}^{-1}$, less than 10 % of the corresponding melt rate in the regular forcing simulation. This finding agrees well with the results of the stand-alone ocean experiments presented earlier in Section 3, where we illustrate that the mean melting response to fast-varying oscillation ocean forcing converges to the mean-state melting response. Likewise, after a spin-up phase of 150 months in represented time, the relative differences in total ocean volume changes between the accelerated and regular forcing simulations remain below 3%, as illustrated in Figure 10b.

https://doi.org/10.5194/gmd-2023-244
Preprint. Discussion started: 9 January 2024

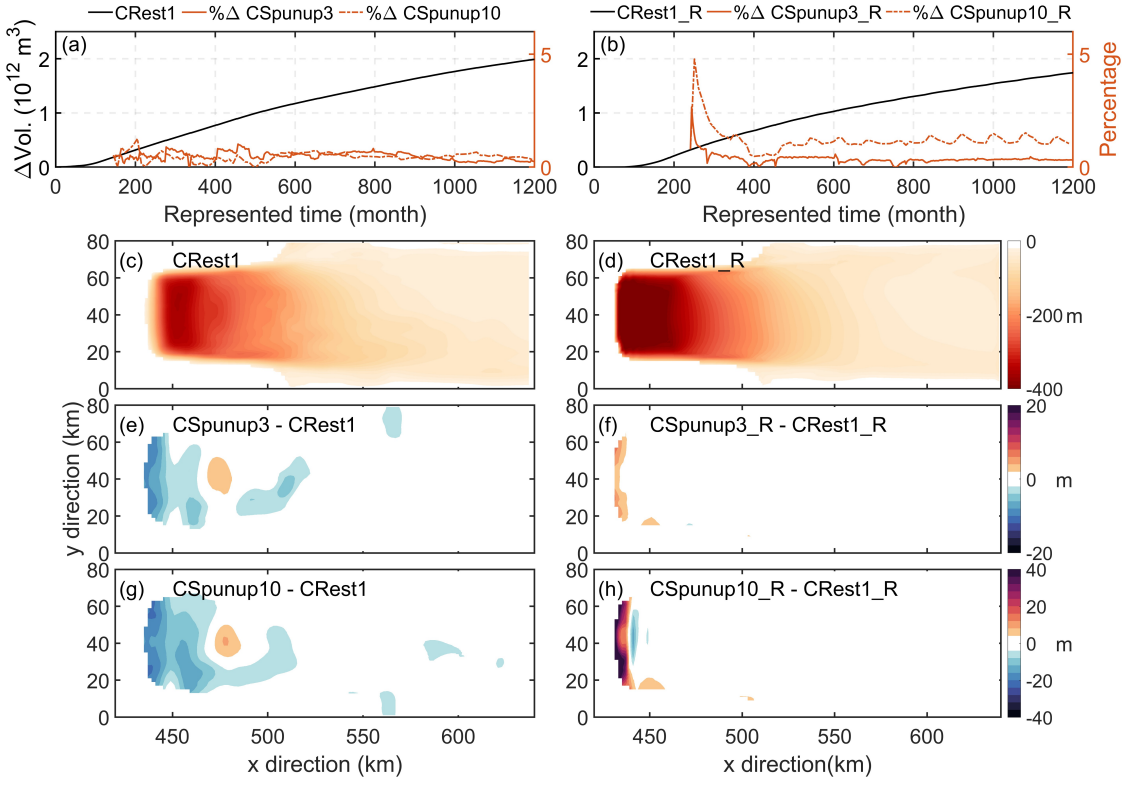

Figure 9. Time series of ocean volume changes from the regular forcing simulation (depicted by black lines) along with absolute differences in percentages in ocean volume changes from both accelerated forcing simulations relative to the regular forcing simultion, derived from (a) the FVCOM-based setup and (b) the ROMS-based setup (b). Panel (c) shows spatial distributions of integrated ice draft changes from the FVCOM-based regular forcing simulation, and panels (e, g) show spatial distributions of difference in integrated draft changes from both FVCOM-based accelerated forcing simulations relative to the regular forcing simulation. Panel (d) shows spatial distributions of integrated ice draft changes from the ROMS-based regular forcing simulation, and panels (f, h) show spatial distributions of difference in integrated draft changes from both ROMS-based accelerated forcing simulations relative to the regular forcing simulation.

https://doi.org/10.5194/gmd-2023-244
Preprint. Discussion started: 9 January 2024

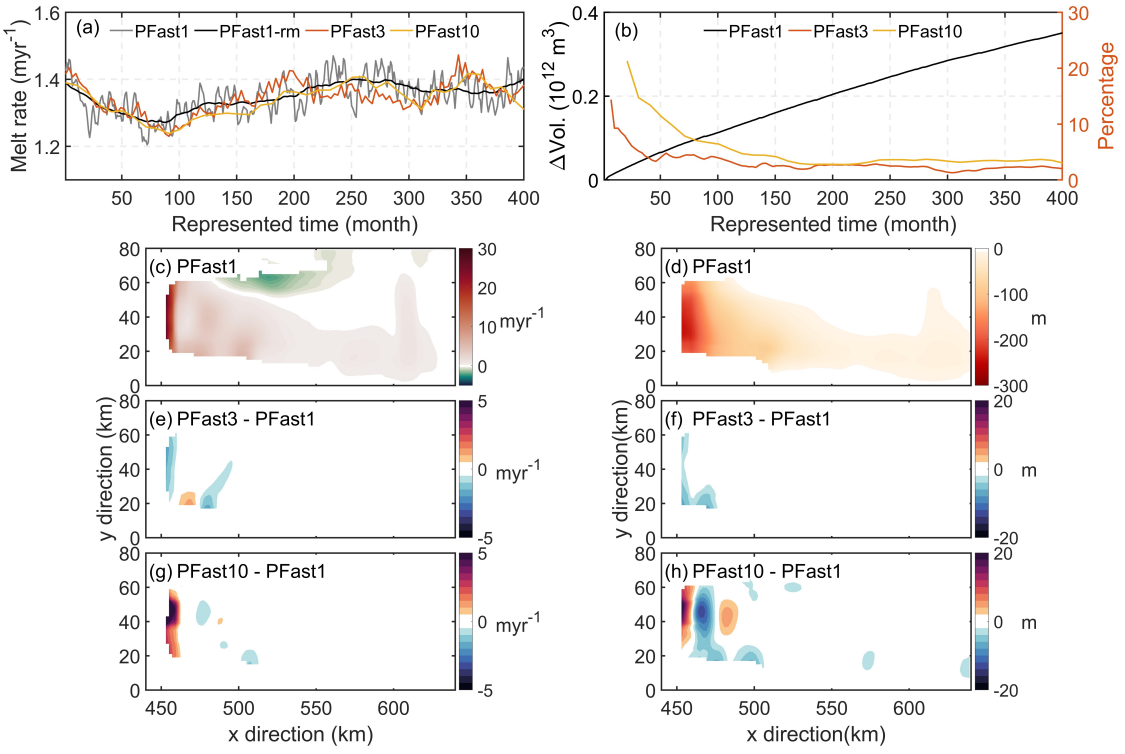

Figure 10. Time series of (a) cavity-averaged melt rates across all simulations in the Periodic-fast class, and (b) ocean volume changes from the regular forcing simulation (depicted by black lines) along with absolute differences in ocean volume changes from both accelerated forcing simulations relative to the regular forcing simulation. Panel (c) shows spatial distributions of melt rates from the regular forcing simulation, and panels (e, g) show spatial distributions of difference in melt rates from both accelerated forcing simulations relative to the regular forcing simulation. Panel (d) shows spatial distributions of integrated ice draft changes from the regular forcing simulation, and panels (f, h) show spatial distributions of difference in ice draft changes from both accelerated forcing simulations relative to the regular forcing simulation.

The spatial pattern in the regular forcing simulation (PFast1) is characterized by enhanced melting near the grounding line reaching up to 30 myr^{-1} (Figure 10c) and an asymmetric pattern of melting at the lower part and freezing at the upper part of the cavity approximately 20 km away from the grounding line. This spatial pattern shows general assemblance as the pattern seen in the stand-alone MEAN forcing simulation (FI_C2M, Figure 3b). Absolute differences in melt rates from both accelerated forcing simulations (PFast3/10) relative to the regular forcing simulation are lower than 0.5 myr^{-1} across most of the cavity, indicated by the large uncolored areas away from the grounding line in Figure 10e and Figure 10g. However, notable deviations in melt rates compared to the regular forcing simulation are observed near the grounding line when using a higher acceleration factor of 10. Here exists a few locations of melt rate differences exceeding 15 myr^{-1}, more than half of that from the regular forcing simulation (Figure 10g).

https://doi.org/10.5194/gmd-2023-244
Preprint. Discussion started: 9 January 2024


Geoscientific Model Development Discussions

As a result of the melting pattern, the most pronounced integrated draft reductions in the regular forcing simulation are observed at the lower flank of the cavity and near the grounding line, reaching 200 m (Figure 10d). Absolute deviations in integrated draft changes from the accelerated forcing simulation with a factor of 3 (PFast 3) relative to the regular forcing simulation are small, below 2 m across most of the cavity, with a few points near the grounding line exceeding 5 m (Figure 10d). In the accelerated forcing simulation with a higher factor of 10 (PFast 10), the absolute deviations increase in the inner part of the cavity (x <500 km), with a few locations exceeding 20 m near the grounding line (Figure 10h). The grounding line positions are consistent across the three simulations at x = 435 km.

In summary, except the relative differences in melt rates and integrated ice draft changes exceed 10% at a few locations in the vicinity of the grounding line when we use a higher acceleration factor of 10, the accelerated forcing simulations can reproduce the time-averaged melting response, total ocean volume changes, spatial distributions of melt rates and integrated ice draft changes, with a relative change of less than 10%. Thus, we consider the accelerated forcing approach to be suitable when the forcing timescale is significantly shorter than the cavity residence time, as suggested by our findings from the stand-alone experiments.

4.2.3 Slow-varying far-field ocean conditions

In the coupled model forced with slow-varying oscillation ocean conditions with a timescale much longer than its CMRT, the regular forcing simulation (PSlow1) displays a temporal melting response with an oscillation pattern of approximately a 30-year period in represented time, as depicted by the black lines in Figure 11a. This pattern reflects the period of ocean forcing in the regular forcing simulation. In the accelerated forcing simulations, although the oscillation period is captured, there is a noticeable reduction in oscillation amplitude, shown by the red and orange lines in Figure 11a. Specifically, in the second cycle, peak melt rates decrease from approximately $5\ \mathrm{myr}^{-1}$ in PSlow1 to about $4\ \mathrm{myr}^{-1}$ in the simulation with an acceleration factor of 1.5 (PSlow1.5), and further to approximately $2\ \mathrm{myr}^{-1}$ with a factor of 3 (PSlow3). This reduction in melting amplitude agrees well with findings from our stand-along experiments presented in Section 3, which indicate that melting decreases when the ocean forcing period is not significantly different from the MCRT. In PSlow3, the 10-year forcing period is not significantly different from the MCRT of 4 years, in contrast to the 30-year period in PSlow1, resulting in significantly reduced melting. In addition, the asymmetrical melt rate curve in PSlow1, which is characterized by a rapidly rising peak, slower decline, and a prolonged period of low melt and relates to internal feedbacks of the cavity circulation with the forcing, becomes less pronounced in PSlow1.5 and almost disappears in PSlow3, as illustrated in Figure 11a. This indicates that the equilibrium response when the forcing period is significantly longer than the CMRT, can not be fully developed in the case of accelerated ocean conditions. Furthermore, Figure 11b reveals significant differences in total ocean volume changes across the three simulations. By the end of the simulation, the total changes amount to $0.62 \times 10^{12}\mathrm{m}^3$, $0.4 \times 10^{12}\mathrm{m}^3$, and $0.18 \times 10^{12}\mathrm{m}^3$ in PSlow1, PSlow1.5, and PSlow3, respectively. This represents relative differences of approximately 35% and 70% in the two accelerated forcing simulations.

The spatial melting pattern in PSlow 1.5 and PSlow3 also notably differs from that in PSlow1. Specifically, Pslow1 exhibits a spatial pattern similar to that observed in the stand-alone MEAN ocean forcing simulation (FI_C2M), manifested as a high-

https://doi.org/10.5194/gmd-2023-244
Preprint. Discussion started: 9 January 2024

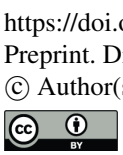

Geoscientific Model Development
Discussions
Open Access
EGU

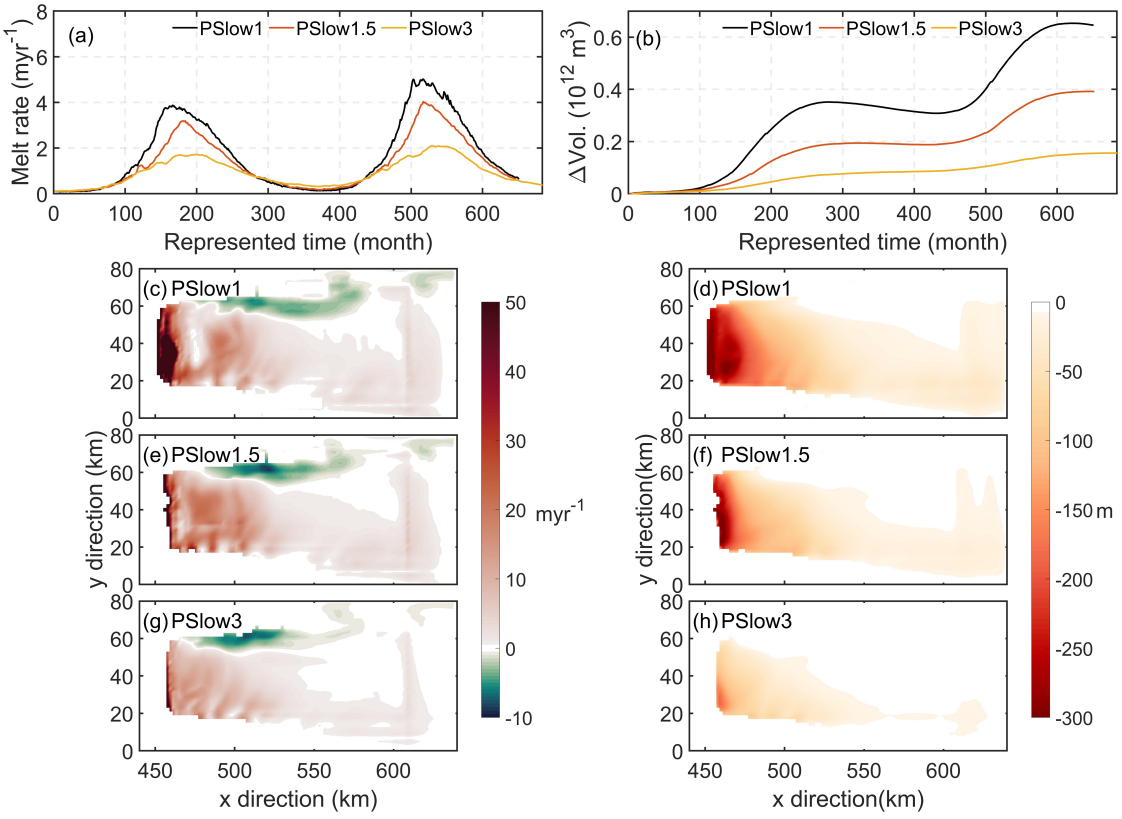

Figure 11. Time series of (a) cavity-averaged melt rates and (b) ocean volume changes across all simulations in the Period-slow class. The first 34 months are considered model spin-up and are excluded from the analysis. Panels (c, e, g) show spatial distributions of melt rates, and panels (d, f, h) show spatial distributions of integrated ice draft changes derived from all simulations.

melting zone exceeding $50\ \mathrm{myr}^{-1}$ near the grounding line and an asymmetric pattern of melting and freezing 20 km away from the grounding line, as shown in Figure 11c. However, this high-melting zone is less evident in PSlow1.5 and PSlow3 (Figure 11e,g). This discrepancy extends to integrated ice draft changes: significant reductions of more than 300 m near the grounding line in PSlow1 (Figure 11 d) are only partially visible PSlow1.5 (Figure 11 f) and nearly absent in PSlow3 (Figure 11 h). The grounding line also retreats less in PSlow3 and PSlow1.5 than in PSlow1, with positions at $x = 455$ km, 451 km, and 445 km, respectively.

In summary, the accelerated forcing simulations, particularly PSlow3, do not effectively replicate the melting response observed in the regular forcing simulation (PSlow1). This is largely attributable to the accelerated timescale of ocean forcing in PSlow3 being close to the mean cavity residence time.

https://doi.org/10.5194/gmd-2023-244
Preprint. Discussion started: 9 January 2024


Geoscientific Model Development Discussions

5 Discussion and conclusions

In this study, we have introduced the accelerated forcing approach to address the discrepancy in timescales between ice sheet and ocean models in coupled modelling. This approach, which extends the ocean simulation duration by a constant acceleration factor, has been evaluated within the MISOMIP1 framework across three scenarios representing varied far-field ocean conditions categorized based on their relation to the mean cavity residence time.

The mean cavity residence time, an intrinsic timescale of the ocean model and mainly determined by the cavity geometry, can be quantified by the stand-alone ocean experiments. It represents the period needed for the cavity to adjust to a steady ocean boundary forcing. When the timescale of unsteady ocean forcing approaches this intrinsic timescale, there will be interactions between basal melting, cavity circulation, the heat inertia within the cavity, and transient changes in the boundary forcing. Consequently, the melting response becomes highly sensitive to any alterations in these factors. This scenario challenges the underlying assumption of the accelerated forcing approach: that basal melting response is not sensitive to corresponding accelerations in ocean boundary forcing. Therefore, the accelerated forcing approach loses effectiveness when the forcing timescale, whether under regular or accelerated forcing approaches, is in the order of the mean cavity residence time.

However, when the ocean forcing varies over a timescale much shorter than the cavity residence time, the ocean model system behaves similarly to a low-pass filter. In this case, the time-average melting response is less coupled with the varying boundary forcing and tends to converge to a stable state produced by the time-averaged forcing, making it insensitive to changes in timescales of the forcing. This scenario upholds the assumption of the accelerated approach. Therefore, in the Fast-varying experiment class, the accelerated forcing approach effectively reproduces the melting response seen with regular forcing.

When the timescale of the ocean forcing significantly exceeds the cavity residence time, the model system has enough time to respond to each forcing phase, allowing the melting to stabilize at an equilibrium state at all phases of the forcing cycle. This process is well elucidated in (Holland, 2017). The same pattern is evident in the melt rate time series from the stand-alone FVCOM-ISOMIP simulation with a 30-year oscillating forcing, where the forcing timescale significantly exceeds the mean cavity residence time of 4 years. We anticipate that for forcings with timescales exceeding 30 years, melting would also reach equilibrium in each phase, with a consistent mean melt rate averaged over the respective cycles. Consider a case in which the forcing timescale is 300 years, 10 times the 30-year period, the melting will reach a similar equilibrium state at every phase of the 300-year cycle, but over a phase period 10 times longer. Therefore, the melting response in any single phase of the 300-year cycle can be reflected by the response in the corresponding single phase of the 30-year cycle. This upholds the fundamental assumption of the accelerated forcing approach. While we haven't tested forcings with oscillation periods longer than 30 years due to resource constraints, the constant forcing in the Constant experiment class essentially represents an infinitely slow varying force once the model reaches a quasi-equilibrium state. Consequently, the accelerated forcing approach successfully replicated the melting response observed under regular forcing in this experiment class, except for ice draft changes and melt rates near the grounding line, which warrant further investigation.

Our study demonstrates that the accelerated forcing approach can be a useful tool in coupled ice sheet-ocean modelling. The approach can directly contribute to the MISOMIP1 project by reducing the required simulation time of 100 years, depending

https://doi.org/10.5194/gmd-2023-244
Preprint. Discussion started: 9 January 2024

on the acceleration factors. Applying the accelerated approach with a factor of 3 for the IceOcean1 experiment has reduced the spun-up simulation duration by a factor of 3 and reproduced most of the melting diagnostics within 10% of those with the regular forcing approach across two participating coupled models. Recommending the accelerated forcing approach to other participating models within the MISOMIP1 framework would provide a more comprehensive understanding of the robustness and applicability of the approach in idealized model setups.

Moreover, there is no reason to believe that the accelerated forcing approach is inapplicable to real-world scenarios. This approach could be applicable in modelling studies related to Antarctica's contribution to sea level rise projections, particularly when the ocean forcing varies over century-long timescales. These timescales vastly exceed the mean cavity residence time of any single ice shelve around Antarctica. For instance, cold-water ice shelves like the Fichner-Ronne Ice shelf and the Ross Ice Shelf have a cavity residence time of approximately 4-8 years (Nicholls and Østerhus, 2004; Loose et al., 2009). Warmer-water ice shelves like those in the Amundsen Sea have even shorter cavity residence times, given their smaller sizes and faster melting-driven cavity circulations. In such cases, the timescales in the accelerated ocean forcing timescales, when applying the approach, would still be significantly longer than the shelves' residence time of a few years, ensuring the effectiveness of the accelerated forcing approach.

Testing across various acceleration factors in the three coupled experiment classes has revealed a trade-off between computational efficiency and integrity in melting response. While higher acceleration factors reduce simulation duration more, they also introduce larger deviations in melting response. This necessitates a careful balance between computational efficiency and the integrity of the modeled melting response.

While we have used a fixed cavity residence time in interpreting our experiment results, the cavity residence time in coupled models varies due to cavity geometry and circulation changes. This poses a challenge when using the accelerated forcing approach: the basal melting integrity maintained for a specific acceleration factor might not hold for another. Time-varying acceleration factors could address the challenge and require exploration in future developments.

Last, we emphasize that applying the accelerated forcing approach and choosing the acceleration factor should be evaluated case-by-case, with careful judgment and sensitivity testing.

Code availability. The FISOC-ROMSIceShelf-Elmer/Ice source code, version information for related software, and input files needed to run the experiments described in the current study are all publicly available (https://doi.org/10.5281/zenodo.5908713).

Author contributions. QZ, RG, and TH conceptualized and designed the study, CZ and BGZ contributed to the experiment design. QZ implemented the experiments using FVCOM, and CZ implemented the experiments using ROMS and Elmer. QZ led the analysis and wrote the initial draft. All authors contributed to the discussion of the results and paper writing.

https://doi.org/10.5194/gmd-2023-244
Preprint. Discussion started: 9 January 2024

Competing interests. The authors declare that they have no conflict of interest.

Acknowledgements. Qin Zhou received financial support from Norwegian Research Council project 295075. Chen Zhao and Ben Galton-Fenzi received grant funding from the Australian Government as part of the Antarctic Science Collaboration Initiative program (ASCI000002). Tore Hattermann acknowledges financial support from Norwegian Research Council project 280727. Rupert Gladstone was supported by Academy of Finland grant numbers 322430 and 355572, and by the Finnish Ministry of Education and Culture and CSC - IT Center for Science (Decision diary number OKM/10/524/2022). David Gwyther was supported by Australian Research Council Discovery Project Grant DP220102525 The authors wish to acknowledge CSC – IT Center for Science, Finland, for computational resources.

https://doi.org/10.5194/gmd-2023-244
Preprint. Discussion started: 9 January 2024

Geoscientific Model Development Discussions
Open Access
EGU

References

Asay-Davis, X. S., Cornford, S. L., Durand, G., Galton-Fenzi, B. K., Gladstone, R. M., Gudmundsson, G. H., Hattermann, T., Holland, D. M., Holland, D., Holland, P. R., Martin, D. F., Mathiot, P., Pattyn, F., and Seroussi, H.: Experimental design for three interrelated marine ice sheet and ocean model intercomparison projects: MISMIP v. 3 (MISMIPC), ISOMIP v. 2 (ISOMIPC) and MISOMIP v. 1 (MISOMIP1), Geosci. Model Dev., 9, 2471–2497, 2016.

Chen, C., Liu, H., and Beardsley, R. C.: An unstructured, finite-volume, three-dimensional, primitive equation ocean model: application to coastal ocean and estuaries., J. Atm. Oceanic Tech., 2003.

Dinniman, M., Klinck, J. M., and Smith, W. O.: Influence of sea ice cover and icebergs on circulation and water mass formation in a numerical circulation model of the Ross Sea, Antarctica, J. Geophys. Res., 112, doi:10.1029/2006JC004036, 2007.

Dutrieux, P., Stewart, C., Jenkins, A., Nicholls, K. W., Corr, H. F., Rignot, E., and Steffen, K.: Basal terraces on melting ice shelves, Geophysical Research Letters, 41, 5506–5513, https://doi.org/10.1002/2014GL060618, 2014.

Edwards, T. L., Nowicki, S., Marzeion, B., Hock, R., Goelzer, H., Seroussi, H., Jourdain, N. C., Slater, D. A., Turner, F. E., Smith, C. J., et al.: Projected land ice contributions to twenty-first-century sea level rise, Nature, 593, 74–82, 2021.

Favier, L., Durand, G., Cornford, S. L., Gudmundsson, G. H., Gagliardini, O., Gillet-Chaulet, F., Zwinger, T., Payne, A., and Le Brocq, A. M.: Retreat of Pine Island Glacier controlled by marine ice-sheet instability, Nature Climate Change, 4, 117–121, 2014.

Favier, L., Jourdain, N. C., Jenkins, A., Merino, N., Durand, G., Gagliardini, O., Gillet-Chaulet, F., and Mathiot, P.: Assessment of sub-shelf melting parameterisations using the ocean–ice-sheet coupled model NEMO(v3.6)–Elmer/Ice(v8.3), Geoscientific Model Development, 12, 2255–2283, https://doi.org/10.5194/gmd-12-2255-2019, 2019.

Foldvik, A., Gammelsrød, T., Østerhus, S., Fahrbach, E., Rohardt, G., Schröder, M., Nicholls, K. W., Padman, L., and Woodgate, R. A.: Ice shelf water overflow and bottom water formation in the southern Weddell Sea, J. Geophys. Res.., 109, C02 015, doi:10.1029/2003JC002008, 2004.

Gagliardini, O., Zwinger, T., Gillet-Chaulet, F., Durand, G., Favier, L., de Fleurian, B., Greve, R., Malinen, M., Martín, C., Råback, P., Ruokolainen, J., Sacchettini, M., Schäfer, M., Seddik, H., and Thies, J.: Capabilities and performance of Elmer/Ice, a new-generation ice sheet model, Geoscientific Model Development, 6, 1299–1318, https://doi.org/10.5194/gmd-6-1299-2013, 2013.

Galton-Fenzi, B. K., Hunter, J. R., Coleman, R., Marsland, S. J., and Warner, R. C.: Modeling the basal melting and marine ice accretion of the Amery Ice Shelf, J. Geophys. Res., 117, C09 031, https://doi.org/10.1029/2012JC008214, 2012.

Gladstone, R., Payne, A. J., and Cornford, S. L.: Resolution requirements for grounding-line modelling: sensitivity to basal drag and ice-shelf buttressing, Annals Of Glaciology, 53, 97–105, https://doi.org/10.3189/2012AoG60A148, 2012.

Gladstone, R., Galton-Fenzi, B., Gwyther, D., , Q., Hattermann, T., Zhao, C., Jong, L., Xia, Y., Guo, X., Petrakopoulos, K., Zwinger, T., Shapero, D., and Moore, J.: The Framework For Ice Sheet–Ocean Coupling (FISOC) V1.1, GMD, 14, 889–905, https://doi.org/10.5194/gmd-14-889-2021, 2021.

Goldberg, D. N., Twelves, A. G., Holland, P. R., and Wearing, M. G.: The nonlocal impacts of Antarctic subglacial runoff, 2023.

Gwyther, D. E., Dow, C. F., Jendersie, S., Gourmelen, N., and Galton-Fenzi, B. K.: Subglacial freshwater drainage increases simulated basal melt of the Totten Ice Shelf, Geophysical Research Letters, 50, e2023GL103 765, 2023.

Hellmer, H. H., Kauker, F., Timmermann, R., Determann, J., and Rae, J.: Twenty-first-century warming of a large Antarctic ice-shelf cavity by a redirected coastal current, Nature, 485, 225–228, https://doi.org/10.1038/nature11064, 2012.

https://doi.org/10.5194/gmd-2023-244
Preprint. Discussion started: 9 January 2024

Holland, P. R.: The Transient Response of Ice Shelf Melting to Ocean Change, Journal of Physical Oceanography, 47, 2101–2114, https://doi.org/10.1175/JPO-D-17-0071.1, 2017.

Holland, P. R., Jenkins, A., and Holland, D. M.: The Response of Ice Shelf Basal Melting to Variations in Ocean Temperature, J. Climate, 21, 2558–2572, https://doi.org/10.1175/2007JCLI1909.1, 2008.

Jenkins, A.: A simple model of the ice shelf–ocean boundary layer and current, Journal of Physical Oceanography, 46, 1785–1803, 2016.

Jenkins, A., Nicholls, K. W., and Corr, H. F. J.: Observation and Parameterization of Ablation at the Base of Ronne Ice Shelf, Antarctica, J. Phys. Oceanogr., 40, 2298–2312, https://doi.org/10.1175/2010JPO4317.1, 2010.

Jourdain, N. C., Mathiot, P., Merino, N., Durand, G., Le Sommer, J., Spence, P., Dutrieux, P., and Madec, G.: Ocean circulation and sea-ice thinning induced by melting ice shelves in the Amundsen Sea, J. Geophys. Res., 122, 2550–2573, https://doi.org/10.1002/2016JC012509, 2017.

Jourdain, N. C., Asay-Davis, X., Hattermann, T., Straneo, F., Seroussi, H., Little, C. M., and Nowicki, S.: A protocol for calculating basal melt rates in the ISMIP6 Antarctic ice sheet projections, The Cryosphere, 14, 3111–3134, 2020.

Lesse, G., Roelvink, J. A., van Kester, J., and Stelling, G.: Development and validation of a three-dimensional morphological model, Coastal engineering, 36, 883–915, 2004.

Li, L., Storms, J., and Walstra, D.: On the upscaling of process-based models in deltaic applications, Geomorphology, 304, 201–213, 2018.

Li, Q., England, M. H., Hogg, A. M., Rintoul, S. R., and Morrison, A. K.: Abyssal ocean overturning slowdown and warming driven by Antarctic meltwater, Nature, 615, 841–847, 2023.

Loose, B., Schlosser, P., Smethie, W. M., and Jacobs, S.: An optimized estimate of glacial melt from the Ross Ice Shelf using noble gases, stable isotopes, and CFC transient tracers, J. Geophys. Res., 114, 15 PP., https://doi.org/200910.1029/2008JC005048, 2009.

Morgan, J. A., Kumar, N., Horner-Devine, A. R., Ahrendt, S., Istanbullouglu, E., and Bandaragoda, C.: The use of a morphological acceleration factor in the simulation of large-scale fluvial morphodynamics, Geomorphology, 356, 107 088, 2020.

Muntjewerf, L., Sacks, W. J., Lofverstrom, M., Fyke, J., Lipscomb, W. H., Ernani da Silva, C., Vizcaino, M., Thayer-Calder, K., Lenaerts, J. T., and Sellevold, R.: Description and Demonstration of the Coupled Community Earth System Model v2–Community Ice Sheet Model v2 (CESM2-CISM2), Journal of Advances in Modeling Earth Systems, 13, e2020MS002 356, 2021.

Nakayama, Y., Cai, C., and Seroussi, H.: Impact of subglacial freshwater discharge on Pine Island Ice Shelf, Geophysical research letters, 48, e2021GL093 923, 2021.

Naughten, K. A., Meissner, K. J., Galton-Fenzi, B. K., England, M. H., Timmermann, R., Hellmer, H. H., Hattermann, T., and Debernard, J. B.: Intercomparison of Antarctic ice-shelf, ocean, and sea-ice interactions simulated by MetROMS-iceshelf and FESOM 1.4, Geoscientific Model Development, 11, 1257–1292, 2018.

Naughten, K. A., De Rydt, J., Rosier, S. H., Jenkins, A., Holland, P. R., and Ridley, J. K.: Two-timescale response of a large Antarctic ice shelf to climate change, Nature communications, 12, 1–10, 2021.

Nicholls, K. W. and Østerhus, S.: Interannual variability and ventilation timescales in the ocean cavity beneath Filchner-Ronne Ice Shelf, Antarctica, Journal of Geophysical Research: Oceans, 109, 2004.

Pelle, T., Morlighem, M., Nakayama, Y., and Seroussi, H.: Widespread Grounding Line Retreat of Totten Glacier, East Antarctica, Over the 21st Century, Geophysical Research Letters, 48, e2021GL093 213, https://doi.org/https://doi.org/10.1029/2021GL093213, e2021GL093213 2021GL093213, 2021.

Pelletier, C., Fichefet, T., Goosse, H., Haubner, K., Helsen, S., Huot, P.-V., Kittel, C., Klein, F., Le clec'h, S., van Lipzig, N. P. M., Marchi, S., Massonnet, F., Mathiot, P., Moravveji, E., Moreno-Chamarro, E., Ortega, P., Pattyn, F., Souverijns, N., Van Achter, G.,

https://doi.org/10.5194/gmd-2023-244
Preprint. Discussion started: 9 January 2024

Vanden Broucke, S., Vanhulle, A., Verfaillie, D., and Zipf, L.: PARASO, a circum-Antarctic fully coupled ice-sheet–ocean–sea-ice–atmosphere–land model involving f.ETISh1.7, NEMO3.6, LIM3.6, COSMO5.0 and CLM4.5, Geoscientific Model Development, 15, 553–594, https://doi.org/10.5194/gmd-15-553-2022, 2022.

Richter, O., Gwyther, D. E., Galton-Fenzi, B. K., and Naughten, K. A.: The Whole Antarctic Ocean Model (WAOM v1.0): development and evaluation, GMD, 15, 617–647, https://doi.org/10.5194/gmd-15-617-2022, 2022.

Schoof, C.: Ice-sheet acceleration driven by melt supply variability, Nature, 468, 803–806, https://doi.org/10.1038/nature09618, 2010.

Seroussi, H., Nakayama, Y., Larour, E., Menemenlis, D., Morlighem, M., Rignot, E., and Khazendar, A.: Continued retreat of Thwaites Glacier, West Antarctica, controlled by bed topography and ocean circulation, Geophysical Research Letters, 44, 6191–6199, https://doi.org/https://doi.org/10.1002/2017GL072910, 2017.

Seroussi, H., Nowicki, S., Payne, A. J., Goelzer, H., Lipscomb, W. H., Abe-Ouchi, A., Agosta, C., Albrecht, T., Asay-Davis, X., Barthel, A., Calov, R., Cullather, R., Dumas, C., Galton-Fenzi, B. K., Gladstone, R., Golledge, N. R., Gregory, J. M., Greve, R., Hattermann, T., Hoffman, M. J., Humbert, A., Huybrechts, P., Jourdain, N. C., Kleiner, T., Larour, E., Leguy, G. R., Lowry, D. P., Little, C. M., Morlighem, M., Pattyn, F., Pelle, T., Price, S. F., Quiquet, A., Reese, R., Schlegel, N.-J., Shepherd, A., Simon, E., Smith, R. S., Straneo, F., Sun, S., Trusel, L. D., Van Breedam, J., van de Wal, R. S. W., Winkelmann, R., Zhao, C., Zhang, T., and Zwinger, T.: ISMIP6 Antarctica: a multi-model ensemble of the Antarctic ice sheet evolution over the 21st century, The Cryosphere, 14, 3033–3070, https://doi.org/10.5194/tc-14-3033-2020, 2020.

Shchepetkin, A. F. and McWilliams, J. C.: The Regional Ocean Modeling System (ROMS): A split-explicit, free-surface, topography-following coordinates ocean model, Ocean Model., 9, 347–404, 2005.

Smith, R. S., Mathiot, P., Siahaan, A., Lee, V., Cornford, S. L., Gregory, J. M., Payne, A. J., Jenkins, A., Holland, P. R., Ridley, J. K., et al.: Coupling the UK Earth System Model to dynamic models of the Greenland and Antarctic ice sheets, Journal of Advances in Modeling Earth Systems, 13, e2021MS002 520, 2021.

Timmermann, R. and Goeller, S.: Response to Filchner–Ronne Ice Shelf cavity warming in a coupled ocean–ice sheet model – Part 1: The ocean perspective, Ocean Sci., 13, 765–776, https://search.proquest.com/docview/1940938744?accountid=17260, 2017.

Van Achter, G., Fichefet, T., Goosse, H., Pelletier, C., Haubner, K., and Pattyn, F.: Ocean–Ice Sheet Coupling in the Totten Glacier Area, East Antarctica: Analysis of the Feedbacks and Their Response to a Sudden Ocean Warming, Geosciences, 13, 106, 2023.

Zhao, C., Gladstone, R., Galton-Fenzi, B. K., Gwyther, D., and Hattermann, T.: Evaluation of an emergent feature of sub-shelf melt oscillations from an idealized coupled ice sheet–ocean model using FISOC (v1.1) – ROMSIceShelf (v1.0) – Elmer/Ice (v9.0), Geoscientific Model Development, 15, 5421–5439, https://doi.org/10.5194/gmd-15-5421-2022, 2022.

Zhou, Q. and Hattermann, T.: Modeling ice shelf cavities in the unstructured-grid, Finite Volume Community Ocean Model: Implementation and effects of resolving small-scale topography, Ocean Modelling, 146, 101 536, https://doi.org/https://doi.org/10.1016/j.ocemod.2019.101536, 2020.